



Mixing of dust aerosols into a mesoscale convective system: Generation, filtering and possible feedbacks on ice anvils

Pierre Tulet, K. Crahan-Kaku, Maud Leriche, Benjamin Aouizerats, Suzanne Crumeyrolle

► To cite this version:

Pierre Tulet, K. Crahan-Kaku, Maud Leriche, Benjamin Aouizerats, Suzanne Crumeyrolle. Mixing of dust aerosols into a mesoscale convective system: Generation, filtering and possible feedbacks on ice anvils. *Atmospheric Research*, 2010, 96 (2-3), pp.302-314. 10.1016/j.atmosres.2009.09.011 . hal-00987566

HAL Id: hal-00987566

<https://hal.science/hal-00987566>

Submitted on 6 May 2014

HAL is a multi-disciplinary open access archive for the deposit and dissemination of scientific research documents, whether they are published or not. The documents may come from teaching and research institutions in France or abroad, or from public or private research centers.

L'archive ouverte pluridisciplinaire **HAL**, est destinée au dépôt et à la diffusion de documents scientifiques de niveau recherche, publiés ou non, émanant des établissements d'enseignement et de recherche français ou étrangers, des laboratoires publics ou privés.

Mixing of dust aerosols into a mesoscale convective system. Generation, filtering and possible feedbacks on ice anvils.[☆]

P. Tulet*

*Meteo-France, CNRM/GAME 42 Gaspard Coriolis 31057 Toulouse, France
LACy, Université de La Réunion, 15 Av René Cassin, 97715 Saint-Denis*

K. Crahan-Kaku

Meteo-France, CNRM/GAME 42 Gaspard Coriolis 31057 Toulouse, France

M. Leriche

*Laboratoire d'Aérodynamique/CNRS, Université de Toulouse 14 av Ed Belin 31400 Toulouse,
France*

B. Aouizerats

Meteo-France, CNRM/GAME 42 Gaspard Coriolis 31057 Toulouse, France

S. Crumeyrolle

Meteo-France, CNRM/GAME 42 Gaspard Coriolis 31057 Toulouse, France

Abstract

During the second Specific Observing Period (SOP) of the African Monsoon Multidisciplinary Analyses (AMMA) campaign, several intense Mesoscale Con-

*Corresponding author

Email addresses: pierre.tulet@meteo.fr (P. Tulet),
katie@atmos.washington.edu (K. Crahan-Kaku), maud.leriche@aero.obs-mip.fr
(M. Leriche), benjamin.aouizerats@cnrm.meteo.fr (B. Aouizerats),
s.crumeyrolle@opgc.univ-bpclermont.fr (S. Crumeyrolle)

vective Systems (MCS) developed over Niger. An examination of a particular convective storm simulated with a mesoscale model near Banizoumbou, Niger, on 1 July, 2006, shows that this MCS generates a strong emission of dust particles at the leading edge of its density current. A fraction of these dust aerosols are uplifted by the convective core of the system and redistributed by aqueous processes. Aerosol impaction scavenging is the main process by which particles are deposited within the mesoscale convective system. However, small particles (smaller than $1\mu m$) that are not efficiently scavenged, are able to reach the upper troposphere at a concentration of 6 particles per cm^3 . This suggests that deep convection over semi-arid regions is able to create its own ice nuclei in high concentrations. This leads to the question: can deep convection over semi-arid regions affect particular ice properties such as ice anvil extension or induce possible feedbacks of dust on precipitation through ice sedimentation?

Key words: dust, aerosol scavenging, ice nuclei, gust front, Mesoscale Convective Systems

1. Introduction

Mineral dust contributes significantly to the global radiative budget calculations through absorption and scattering of longwave and shortwave radiation (Houghton et al., 2001), and its indirect effect on cloud microphysics (IPCC, 2007), (Twomey, 1959), (Albrecht, 1989), (Sandu et al., 2008)). At a local level, high dust concentrations are shown to impact the vertical structures of storms (Lohmann and Diehl, 2006) and local energy budgets (Grini et al., 2006). The dust diameters have a large range in size, from below

9 0.2 to 40 μm , implying that different sink mechanisms need to be correctly
 10 modeled, such as sedimentation, wet and dry deposition. Dry deposition
 11 includes turbulent transfer to the surface and gravitational settling. Wet
 12 deposition includes nucleation scavenging and impaction scavenging, both
 13 involving complex microphysical interactions between aerosols and hydrometeors.
 14 Nucleation scavenging describes the activation of aerosols into cloud
 15 droplets and ice crystals and subsequent growth to precipitating hydrometeors.
 16 Impaction scavenging is the collection of the aerosols by cloud droplets,
 17 ice crystals and precipitating hydrometeors through Brownian motion, interception,
 18 inertial impaction, thermophoresis, diffusiophoresis, airflow
 19 turbulence and electrostatic attraction in and below the cloud layer (Andronache,
 20 2003). Usually, impaction scavenging by iced hydrometeors are
 21 not considered in numerical models because of its low effect compared to
 22 collection by liquid particles. Theoretically, impaction scavenging is usually
 23 split into two processes: in-cloud impaction scavenging that treats the
 24 interactions between cloud droplets and raindrops with interstitial aerosol
 25 particles, and below cloud scavenging that concerns the collection of aerosol
 26 particles by falling raindrops below the cloud base. The relative importance
 27 of in-cloud scavenging processes (nucleation and impaction scavenging), also
 28 called washout, and below cloud scavenging, also called rainout, depends
 29 on meteorological conditions and on the properties of aerosol particles (size
 30 distribution and chemical composition) as well as on the stage of cloud development.
 31 Global models have estimated that wet deposition only accounts
 32 for 10% of the total dust loss globally (Tegen and Lacis, 1996; Ginoux et al.,
 33 2001). Locally, wet deposition can be expected to play a larger role in dust

removal processes, especially in areas of intense convection, as observed during the monsoon season in West Africa.

The data acquired in the framework of the 2006 African Monsoon Multidisciplinary Analyses (AMMA) field campaign (Redelsperger et al., 2006) provides an excellent opportunity to analyze the processes of dust generation and deposition associated with convection. Within semi-arid regions, the strong winds associated with gust fronts of Mesoscale Convective Systems (MCSs) generate dust and aerosol lofting. Some recent studies have detailed the dust formation in the leading edge of the density current observed in the intertropical discontinuity region (Flamant et al., 2007, 2009; Marsham et al., 2008). The dust generation associated with the 1 July, 2006 MCS (SOP 2 of the AMMA campaign) was modeled near the Niamey and Banizoumbu region (Niger) and compared to observations by Crumeyrolle et al. (2008). The present work is an extension of the Crumeyrolle et al. (2008) study with a special focus on the generation and the vertical transport of dust in the convective core of a MCS in relation to precipitation. In particular, several aspects of a MCS over a semi-arid region that can cause feedbacks of dust on ice in the upper troposphere are emphasized.

2. Model Description

2.1. General parameterizations

The MesoNH model has been jointly developed by the CNRM (Météo-France and Centre National de la Recherche Scientifique) and Laboratoire d'Aérodynamique (Centre National de la Recherche Scientifique and Université de

58 Toulouse) (Lafore et al., 1998). MesoNH simulates small scale atmospheric
 59 circulation (horizontal resolution of a few meters) to synoptic scale (hori-
 60 zontal resolution of several tens of kilometers) and can be run in a two-way
 61 nested mode involving up to 8 nesting stages. Parameterizations have been
 62 introduced for convection (Bechtold et al., 2001), cloud microphysics (Pinty
 63 and Jabouille, 1998; Cohard and Pinty, 2000), turbulence (Bougeault and
 64 Lacarrere, 1989), biosphere-atmosphere thermodynamic exchanges (ISBA)
 65 (Noilhan and Mahfouf, 1996), urban-atmosphere interactions (Masson, 2000),
 66 lightning processes (Barthe et al., 2005), gaseous chemistry (Suhre et al.,
 67 1998; Tulet et al., 2003) and aerosols chemistry (Tulet et al., 2006).

68 *2.2. Mineral dust parameterization*

69 Mineral dust emissions are parameterized following Grini et al. (2006). In
 70 this parameterization, the three lognormal modes are generated and trans-
 71 ported by the ORILAM lognormal aerosol scheme (Tulet et al., 2005). Re-
 72 garding emission processes, dust aerosols are mobilized using the Dust En-
 73 trainment and Deposition model (DEAD) (Zender et al., 2003) which calcu-
 74 lates dust fluxes from wind friction speeds. The physical basis of the model
 75 is taken from Marticorena and Bergametti (1995) in which dust fluxes are
 76 calculated as a function of saltation and sandblasting processes. Here, the
 77 emission of dust aerosols is calculated directly from ISBA surface parameters,
 78 and then sent to the atmosphere consistently with the fluxes of momentum,
 79 energy and humidity. The initial dust size distribution contains three modes
 80 with median radii of 0.32, 1.73 and 4.33 μm and standard deviations of 1.7,
 81 1.6 and 1.5, respectively as defined by Alfaro and Gomes (2001).

82 2.3. The ICE3 cloud microphysics scheme

83 The study uses the ICE3 cloud microphysics scheme described by Pinty
84 and Jabouille (1998). This scheme follows the approach of Lin et al. (1983)
85 in that a three-class ice parameterization is coupled to a Kessler's scheme
86 for warm processes. It is a bulk single moment scheme that predicts the
87 evolution of the mixing ratios of six water species (vapor, cloud droplets
88 and raindrops, pristine ice, snow and graupel). Pristine ice crystal are here
89 assumed to be plates. The precipitation of water drops and ice crystals is
90 parameterized according to Caniaux et al. (1994). The size distribution of the
91 hydrometeors is assumed to follow a generalized γ -law function in normalized
92 form. Due to the use of a single moment bulk scheme, this study does not
93 consider the cloud condensation nuclei and ice nuclei activation. There is
94 no interaction between the dust particles and the microphysics within the
95 model.

96 2.4. Impaction scavenging and aerosol-cloud interactions

97 The impaction scavenging of aerosols is calculated in MesoNH based upon
98 first order principals. In- and below-cloud impaction scavenging by cloud
99 droplets and raindrops uses a kinetic approach to calculate the aerosol mass
100 transfer as:

$$\frac{dM_p}{dt} = -\Lambda_M M_p \quad (1)$$

101 where dM_p/dt represents the aerosol dry mass transfer in the aqueous phase,
102 M_p the aerosol dry mass and Λ_M the path normalized scavenging coefficient in
103 s^{-1} . For impaction scavenging by cloud droplets, the main process to consider
104 is the Brownian motion of dry aerosols and cloud droplets (Pruppacher and

105 Klett, 2000) leading to the normalized scavenging coefficient determined by
 106 the semi-empirical formulation as:

$$\Lambda_M M_p = \frac{1.35 LWC D_p}{r_{cloud}^2} \quad (2)$$

107 where LWC is the cloud liquid water content in $g.cm^{-3}$, D_p is the diffusivity
 108 of the particle in $m^2.s^{-1}$ and r_{cloud} the cloud droplet radius in m .

109 The impaction scavenging by raindrops depends mainly on Brownian motion,
 110 interception, and inertial impaction following a formula originally described
 111 by Slinn (1983):

$$\Lambda_M M_p = \frac{3}{2} \frac{E}{r_{rain}} . F_{rain} \quad (3)$$

112 where E is the collection efficiency fully described in Seinfeld and Pandis
 113 (1997); Tost et al. (2006), r_{rain} the radius of the rain droplets in mm and
 114 F_{rain} the effective precipitation flux in $kg.m^{-2}.s^{-1}$.

115 Within this impaction scavenging scheme, the efficiency is calculated for
 116 three types of collection. Small particles are collected efficiently by raindrops
 117 and cloud droplets through Brownian diffusion, but the collection efficiency
 118 decreases with increasing particle size. Inertial impaction by raindrops is
 119 important for large particles, with collection efficiencies approaching one for
 120 particles with diameter greater than $20 \mu m$. Inside the cloud, impaction scav-
 121 enging by cloud droplets is less efficient for particles with diameters from 0.2
 122 to $2.0 \mu m$. Indeed interception by raindrops is difficult since particles follow
 123 the streamlines of air around the falling droplets. The in-cloud mass aerosol
 124 transfer into rain droplets by autoconversion and accretion processes have
 125 been introduced as described by Pinty and Jabouille (1998). The sedimen-
 126 tation of aerosol mass included in raindrops is solved using a time splitting

127 technique with an upstream differencing scheme of the vertical flux as:

$$P_{asr} = \frac{m_{aero}}{m_{rain}\rho} \frac{d}{dz} (V_r \cdot \rho \cdot r_{rain}) \quad (4)$$

128 where P_{asr} is the raindrops aerosol mass sedimentation rate, m_{aero} the aerosol
 129 mass included in raindrops in $kg.kg^{-1}$, m_{rain} the rain water mass in $kg.kg^{-1}$,
 130 ρ the air density and V_r the raindrop sedimentation velocity in $m.s^{-1}$.

131 As for the microphysical scheme, only mass transfer between aerosols and
 132 warm cloud processes have been considered here. As a consequence the
 133 model follows the aerosol mass of each lognormal mode during its evolution
 134 through the warm ICE3 processes. Indeed the aerosol scheme is limited to one
 135 moment (mass) during its warm processes exchange. This limitation involves
 136 two assumptions: (1) Mass transfer does not change the size distribution of
 137 the aerosol modes, and (2) the rerelease of aerosols into the air due to rain
 138 evaporation is proportional to the mass of water evaporated (Chin et al.,
 139 2000). As a consequence, the mean radii and standard deviation of the
 140 raindrops aerosol modes are identical to the dry aerosol size distribution,
 141 implying that neither coagulation nor chemical transformation occurred in
 142 the cloud droplets are considered in the model. The second assumption
 143 however, is likely to overestimate the release of aerosols due to evaporation
 144 as some evaporation of the rain results in smaller raindrops that still contain
 145 the aerosols.

146 2.5. Model configuration

147 The simulation begins at 00 UTC on June 29, 2006, and ends at 00
 148 UTC on July 2, 2006. Three two-way nested domains are used. The large
 149 domain at 36 km resolution (3.1°S - 31.7°N; 25.64°W - 35.64°E) gives a

150 large scale synoptic view of west Africa. The first embedded domain (12 km
 151 resolution) is centered over northwest Nigeria and covers a large part of the
 152 AMMA campaign area (4.3°N - 17.6°N; 4.19°W - 16.24°E). The embedded
 153 smallest domain at 3 km resolution (11.80°S - 16.82°N; 0.10°W - 8.31°E)
 154 gives a fine scale view of Niger. For the two larger domains, the Bechtold
 155 et al. (2001) convection scheme is used, whereas deep convection is assumed
 156 to be explicitly resolved at 3 km resolution. Only the smallest domain is
 157 examined in this study. The vertical grid is composed of 60 stretched vertical
 158 levels reaching the altitude of 34,000 meters above ground level (m agl); 30
 159 levels are located in the boundary layer between the surface and 2,000 m agl.
 160 Initialization and lateral boundary conditions of the large domain are taken
 161 from the ECMWF analysis.
 162 Two types of simulations have been performed. The complete simulation
 163 (SCAV) uses the dust scavenging scheme whereas the NOSCAV simulation
 164 do not include wet deposition for dust. Because there is no connection of
 165 dusts with dynamics and microphysics, these two simulations give identical
 166 MCSs. Actually, the difference between these two simulations shows the
 167 impact of precipitation on the dust distribution.

168 **3. Mesoscale convection and dust generation**

169 This section focus on the vertical structure of a MCS observed and simu-
 170 lated east of Banizoumbou the 1st of July at midnight. Figures 1.a, 1.c and
 171 1.e display the MSG brightness temperature (at 10.8 μm) on 1 July 2006 at
 172 18 UTC, 2 July at 00 UTC and 2 July at 02 UTC, respectively (Chaboureaux
 173 and Pinty, 2006). The MSG satellite images show the passage of several con-

174 vective systems over the south-east of Niger: most of the MCSs are triggered
 175 at the eastern part of the simulated domain (Fig. 1.a) and propagate to the
 176 west over the Niamey and Banizoumbou region. The two most intense sys-
 177 tems are observed north of and over Banizoumbou between 00 UTC and 02
 178 UTC (Fig. 1.c and 1.e). The northern MCS is triggered 3° north-east of Ban-
 179 izoumbou (Fig. 1.a) and propagates to Niamey and Burkina Faso (Fig. 1.c
 180 and 1.e). The second system is triggered at 2.5° east of Banizoumbou (Fig.
 181 1.a). It moves slowly (Fig. 1.c) and disappears over Banizoumbou (Fig. 1.e).

182
 183 Figures 1.b, 1.d and 1.f give the cloud top height (dashed) and the in-
 184 stantaneous precipitation (isolines) simulated by MesoNH on 1 July 2006 at
 185 16 UTC, 18 UTC and 20 UTC, respectively. As observed previously on the
 186 satellite images, some convective systems are simulated over the south-east
 187 of Niger where the two main systems have reached the Niamey region. The
 188 system north is triggered on 1 July 2006 at 16 UTC, at 1° north-east of
 189 Banizoumbou (Fig. 1.b). This difference in the initiation location will cause
 190 a 5 hours time lag in the passage of the systems over the Niamey and Ban-
 191 izoumbou region. However it evolves similarly to observations, except for
 192 passing a bit too south of Niamey (Fig. 1.c, 1.d, 1.e and 1.f). The southern
 193 system begins 2.5° east of Banizoumbou at the same location as observed
 194 on the MSG images, but one hour earlier than observed (Fig. 1.a and 1.b).
 195 Furthermore, its propagation is quite different from the observed MCS. At
 196 20 UTC, the system is simulated 1° southeast of Banizoumbou (Fig.1.d) and
 197 instead of disappearing on Banizoumbou (Fig. 1.e), the system continues its
 198 propagating to the border of Burkina-Fasso (Fig. 1.f).

199 The overshoot of the modeled MCS reaches 19,000 m agl in the lower strato-
 200 sphere and the top of the anvil is simulated at 16,000 m agl at the altitude of
 201 the tropopause. The area of detrainment is spread over a large area located
 202 at the tropopause. By comparison between the MSG images and the simula-
 203 tion, one can observe that differences exists in the location of triggering and
 204 in the stage of the cycle life. However, these differences should not strongly
 205 affect the focus of this article; the major features of these MCS are realistic
 206 enough and characteristic of convection systems over west Africa.

207 The instantaneous simulated precipitations (isolines) have been superim-
 208 posed to the altitude of the cloud top (isolines on Fig. 1.b, 1.d and 1.f).
 209 The maximum of observed precipitation gives the cloud zone where the con-
 210 vection is strong. The cell simulated at the south-east of Banizoumbou at 20
 211 UTC (Fig 1.d) is particularly active with the precipitation rate reaching 50
 212 $mm.h^{-1}$ at the surface.

213 MCS downdrafts create a gust front where surface winds exceed $15 m.s^{-1}$.
 214 This gust front can be seen on Figure 2 by surface winds vector divergence
 215 in the front of each MCS. The associated surface winds are greater than the
 216 wind speed threshold of $6.5 m.s^{-1}$ for soil erosion determined by Chomette
 217 et al. (1999) over Sahelian-Saharan regions. However, around the MCSs, the
 218 surface winds are low (less than $5 m.s^{-1}$) and they cannot produce dust emis-
 219 sion (Fig. 2). As a consequence, only in the MCS gust front, winds are for
 220 the most part strong enough to move soil particles by saltation and generate
 221 high dust concentration at the surface as simulated by the model ahead and
 222 west of the MCS (Fig.2). More than $10,000 \mu g.m^{-3}$ of dust are simulated
 223 at the surface east of Banizoumbou and $5,000 \mu g.m^{-3}$ over Niamey. Three

others gust fronts with high dust concentration are simulated in the northern part of the domain. They are created by the small convective cells simulated at 19 UTC (not shown) and 20 UTC (Fig. 1.d). Note that the intense dust plume formed in this northern area, is mainly due to the soil characteristics and to the absence of any vegetation.

Simulation validation through observation data was detailed by Crumeyrolle et al. (2008): it was shown that the increase of the surface wind speed, the decrease of surface pressure and the measured precipitation at the arrival of the MCS are correctly reproduced over Niamey. In addition, the dust mass concentration profile in the lower troposphere simulated over the Niamey region before and after the MCS passage are closed to the ATR42 aircraft observations. The next section of the paper focuses on a particular cell which was simulated at the east of Banizoumbou (Fig.2). This cell is significant in the high concentration of dust contained in the gust front (about $3,000 \mu g.m^{-3}$) and the associated precipitation rate is important ($50 mm.h^{-1}$). Furthermore, this cell generates considerable levels of detrainment in the upper troposphere as shown in Figure 1.d.

4. Dust formation and redistribution in the convective cloud

Figure 3 gives the vertical cross section of the total condensed water by the solid line delineated on the Figure 2 (the left corner of the cross section corresponds to the south west point of the solid line). The simulated vertical velocity reached $20 m.s^{-1}$ between 9,000 m agl and 15,000 m agl, (black isolines of Fig. 3), that represents the convective core of the system. More than $2.5 g.kg^{-1}$ of condensed water is simulated within this convective core.

248 Detrainment of the system is modeled at the tropopause located at 16,000
 249 m agl. The convective overshoot reaches 19,000 m agl and transports to the
 250 lower stratosphere more than 1 g.kg^{-1} of total condensed water. Above 6,000
 251 m agl, rainfall appears with a maximum of 4 g.kg^{-1} at 2,000 m agl under
 252 the convective core.

253 This intense precipitation (evaporation and drag of hydrometeors) plays an
 254 important role in the downdrafts and the cold pool formation at the sur-
 255 face. This cold pool is characterized by low potential temperature (298 K),
 256 7 degrees lower than its environment and a negative buoyant air (Fig. 4.a).
 257 However, at the leading edge of the gust front identified by the surface winds
 258 convergence (streamlines in Figure 4.a), the vertical gradient of potential
 259 temperature is null between the surface and 2,000 m agl, showing that the
 260 air of this frontal region is mixed in this layer. Within the cold pool and the
 261 frontal zone, the turbulent kinetic energy modeled is greater than $2 \text{ m}^2.\text{s}^{-2}$
 262 (shaded area on Figure 4.a). Indeed the air from the gust front is mixed by
 263 turbulence in the frontal zone and the winds convergence has forced the air
 264 to rise dynamically above the gust front.

265 Figure 4.b gives the vertical cross section of the dust concentration (SCAV
 266 simulation). On the right side of this Figure, the Sahelian boundary mixing
 267 layer appears with about $200 \text{ }\mu\text{g.m}^{-3}$ of dust. High surface winds associated
 268 with the gust front (more than 12 m.s^{-1} at 10 m agl) generate sandblasting
 269 and a saltation flux of dust particles at the surface (Figure 4.b). Within
 270 the cold pool, $1,500 \text{ }\mu\text{g.m}^{-3}$ of dust is simulated in the complete simula-
 271 tion (SCAV) of Figure 4.b. At the leading edge of the gust front, dust is
 272 transported upward in the ascending current and entrained into the cloud.

273 Knippertz et al. (2009) have also found similar results where strong emission
 274 of dust have been engendered by density current associated to moist convec-
 275 tion over the Atlas Mountains. This entrainment of dusty air in the cloud is
 276 also visible by the curvature of the streamlines of Figure 4.a. Precipitations
 277 (marked by the shaded area of Figure 4.b) scavenges most of the dust mass
 278 concentration entrained into the cloud. They also contributes to decreases
 279 significantly the dust concentration simulated in the cold pool: the maximum
 280 of rain mixing ratio at the surface (2 g.kg^{-1}) corresponds to a local minimum
 281 of dust concentration. Moreover, beyond this maximum, a second band of
 282 precipitation (1 g.kg^{-1}) corresponding to a cumulus simulated in front of the
 283 MCS, also contribute to limit the dust concentration at the east part of the
 284 gust front. Despite of these precipitations, in the SCAV simulation, 500 and
 285 $100 \text{ } \mu\text{g.m}^{-3}$ of these fresh particles produced in the gust front remains at
 286 1,000 m agl and 3,000 m agl, respectively. Dust concentrations decreases to
 287 $30 \text{ } \mu\text{g.m}^{-3}$ at 6,000 m agl (not shown). Flamant et al. (2007) and BouKaram
 288 et al. (2008) showed that the frontal zones like the inter-tropical discontinu-
 289 ity are favorable to dust lifting through turbulence. At a more local scale
 290 and over desert, gust fronts associated to single convection cell, also generate
 291 dust particles and transport aerosols above the boundary layer.
 292 Without any dust scavenging (NOSCAV simulation), the modeled dust con-
 293 centration is much larger, reaching $3000 \text{ } \mu\text{g.m}^{-3}$ in the gust front (Fig. 5).
 294 Convection lifts more than $300 \text{ } \mu\text{g.m}^{-3}$, $100 \text{ } \mu\text{g.m}^{-3}$ and $50 \text{ } \mu\text{g.m}^{-3}$ of dust
 295 formed in the gust front to 5,000 m agl, 10,000 m agl, and 16,000 m agl,
 296 respectively. At the tropopause, these particles are detrained far from the
 297 convective core in the anvil.

298 Figure 6 shows the differences between the dust mass concentration of the
 299 two simulations NOSCAV and SCAV. In both simulations, the dynamics and
 300 cloud microphysics are the same. In-cloud, the differences of dust mass con-
 301 centration between the two simulations (NOSCAV-SCAV) are on the same
 302 order of magnitude as the dust concentration simulated in the NOSCAV
 303 simulation, showing that the dust mass is close to zero in the cloud of the
 304 simulation SCAV. This implies that most of the dust mass concentration has
 305 been scavenged by raindrops. Indeed, with dust scavenging, less than 1500
 306 $\mu g.m^{-3}$ of dust is modeled in the cold pool and as little as 15 $\mu g.m^{-3}$ is able
 307 to reach 8,000 m agl. Furthermore, some notable differences are modeled in
 308 the rain and cloud evaporation zones at the rear part of the MCS. Some of the
 309 dust particles collected by cloud droplets and raindrops are re-released in the
 310 SCAV simulation in the evaporative zones where the precipitation does not
 311 reach the surface. It results in more than 200 $\mu g.m^{-3}$ of dust mass near the
 312 surface due to precipitation evaporation. This can be observed behind the
 313 MCS and during the dissipation stage (Figure 6). Note that these released
 314 dust particles have likely enhanced hygroscopic properties caused by soluble
 315 materials within the monsoon flux coating the mineral dust (Levin et al.,
 316 1996; Crumeyrolle et al., 2008). Indeed, precipitations serve contradicting
 317 purposes: it washes out most of the dust mass in the gust front, but it play
 318 also a major role in the production of fresh dust.

319 **5. Dust vertical distribution and aerosol size filtering**

320 The profile of mass and number concentration for the three dust modes
 321 are plotted in Figure 7 along the cross section of Figure 6 indicated by the

322 vertical dashed line. Note that this profile corresponds to the convective
 323 region of the MCS except between 3,000 m agl and 8,000 m agl where the
 324 profile is at the boundary of the cloud which is indicated by a decrease in
 325 the plotted dust concentration. The vertical profile of the smaller mode with
 326 the median radius of $0.32 \mu m$ is the same for both SCAV and NOSCAV
 327 simulations (green solid and dashed lines are superimposed on Figure 7). It
 328 indicates that this mode is not affected by impaction scavenging since these
 329 particles are too large to be collected by Brownian motion and too fine to
 330 have significant inertial velocities (i.e. collection by inertial impaction). The
 331 collection efficiency factor is less than 0.5 % for the smallest particles mode
 332 whereas for the two larger ones (with median radii of $1.73 \mu m$ and $4.33 \mu m$)
 333 the efficiency factors are 30 and 99 % respectively. As a consequence, the
 334 majority of the dust concentration of the two larger modes has been scav-
 335 enged and 99 % of the mass of the smallest mode is preserved and is able
 336 to be transported upward in the convective core. The vertical profile of Fig-
 337 ure 7.a shows that the precipitation decreases the dust mass concentration
 338 above 2,000 m agl from $150 \mu g.m^{-3}$ ($R_g = 1.73 \mu m$ and $R_g = 4.33 \mu m$) to
 339 $30 \mu g.m^{-3}$ ($R_g = 1.73 \mu m$) and $8 \mu g.m^{-3}$ ($R_g = 4.33 \mu m$). Between 3,000 m
 340 agl and 9,000 m agl, a local maximum of the two larger modes is observed in
 341 the SCAV simulation and corresponds to a local minimum of the NOSCAV
 342 simulation. As explained before, this area is at the boundary of the cloud and
 343 this local maximum corresponds to evaporated rain and cloud droplets that
 344 re-release some new dusts. In the upper troposphere above 15,000 m agl, the
 345 mass concentration from the SCAV simulation reaches respectively $6 \mu g.m^{-3}$
 346 ($R_g = 0.33 \mu m$), $0.8 \mu g.m^{-3}$ ($R_g = 1.73 \mu m$) and $0.4 \mu g.m^{-3}$ ($R_g = 4.33$

μm) whereas the total mass concentration modeled in the NOSCAV simulation is $50 \mu g.m^{-3}$. Indeed, within the SCAV simulation the majority of the mass transported near the tropopause is due to the first mode, representing 80 % of the total mass, whereas this mode represents only 10 % of the total emitted mass.

Even though most of the aerosol mass has been scavenged, the number of small particles reaching higher altitudes still are significant within the SCAV simulation (Figure 7.b). The SCAV simulation shows that 20 particles per cm^3 have been transported to 7,000 m agl and more than 6 particles per cm^3 reach the tropopause (16,000 m agl). This represents 1 to 2 % of the number concentration modeled at the surface in the gust front whereas only 0.4 % of the mass concentration in the gust front reach the upper troposphere.

These results show that the MCS precipitations are two-fold. Firstly, rainfall (drag of hydrometeors and evaporation) is one of the main mechanism that generates downdrafts and causes the formation of a gust front. When convection is located over a dust source region, dust particles are formed in the cold pool, ahead of the precipitation zone, where the soil is dry enough. The size distribution of the emitted dust depends on the wind friction at the surface and thus is also influenced by surface conditions and by the intensity of downdrafts. That is as the emitted dust modes are strongly dependent on the energy of impaction during the sandblasting (Alfaro and Gomes, 2001): the stronger the surface wind, the greater the respective concentration of the smallest particles. A part of these fresh aerosols, which are located at the leading edge of the cold pool, can be entrained in the cloud updraft. Secondly, rainfall filters the size distribution of particles by preserving the first

mode and scavenging the two larger modes. Our model shows that a large number of small particles can be transported by convection. In this case study, more than 6 particles per cm^3 reached the tropopause.

6. Dust transport in the UTLS

On July, 2 at 00 UTC (Figure 1), the simulation shows that the upper level of the MCS detrainment is modeled at 16,000 m agl at the tropopause. At this altitude, more than 6 dust particles per cm^3 have been transported up to the convective core of each MCS (Fig. 8.a). High dust concentration up to $0.2\text{ }cm^{-3}$ are spreading over the main part of the south-west of Niger. The previously studied MCS gets the most intense plume dust concentration: more than $2\text{ }cm^{-3}$ of dust particles have been modeled on a surface exceeding $22,500\text{ }km^2$. Figure 8.b shows that in the lower stratosphere (at 20,000 m agl) the overshoot of the most intense MCS can transport high concentration of dust particles (with maxima reaching over $0.1\text{ }cm^{-3}$). As for water vapor, it is known that convection is an important source of aerosol in the lower stratosphere. For the first time, IN concentration was measured during the CRYSTAL-FACE campaign in Florida (Prenni et al., 2007) using a continuous flow diffusion chamber sampling residual particles remaining after evaporation of cloud particles initially collected by a counterflow virtual impactor. These measurements were made onboard the citation aircraft in anvil of convective clouds at altitudes between 8 and 11 km corresponding to the upper troposphere in Florida. In this study, the range of measured IN concentration is 0.001 to $1\text{ }cm^{-3}$ whereas it is 0.2 to $6\text{ }cm^{-3}$ in the simulated MCS in the upper troposphere over Africa. This suggests that the

396 order of magnitude of aerosol produced and transported by the MCS over
397 African semi-arid regions are high and greater than over Florida (DeMott
398 et al., 2003).

399 7. Conclusion

400 This study emphasizes several important aspects of dust emissions which
401 can be formed in the gust front of a MCS over semi-arid region. In the sim-
402 ulations, this process models dust concentrations greater than $3000 \mu g.m^{-3}$
403 at the surface. Without wet dust scavenging (NOSCAV), about $50 \mu g.m^{-3}$
404 of dust is transported in the convective core and reaches the tropopause,
405 whereas less than $1 \mu g.m^{-3}$ is modeled in the complete simulation (SCAV).
406 Indeed, precipitations filter the main part of the super-micronic dust mode
407 and the sub-micronic mode (here at a median radius of $0.32 \mu m$) is preserved.
408 This mode represents 10 % of the emitted mass but 98 % of the aerosol
409 number. A large number of dust particles reaches the tropopause, with a
410 maximum of 6 particles per cm^3 at 16,000 m agl. This number concentration
411 is several orders of magnitude greater than ice nuclei observed over Florida
412 during the CRYSTAL-FACE campaign where there is no local dust emissions
413 comparable from a semi-arid region. Considering that mineral dust can serve
414 as good ice nuclei (Kanji and Abbatt, 2006; Richardson et al., 2007), the dust
415 generated by convection may influence the ice number concentration near the
416 tropopause. It is assumed that if high ice nuclei concentrations are able to
417 significantly decrease the supersaturation in the section of cloud containing
418 ice, we can expect that dust can play an important role in the type of ice
419 crystals (Nelson, 2001). It is also possible that the modification of the size

420 and type of ice crystals can also affect the lifetime of anvils and impact the
 421 convective precipitation (Gilmore et al., 2004b) through the ice sedimenta-
 422 tion velocity in the upper troposphere. Another study from Gilmore et al.
 423 (2004a) compared cloud resolving model simulations results using liquid-only
 424 and liquid and ice phase microphysics. They underlined the role of the ice
 425 phase in increasing precipitation production aloft and producing stronger
 426 downdrafts and greater low-level downward precipitation fluxes (and ground
 427 accumulations) compared to liquid-only simulations. In addition, the varia-
 428 tion of ice-forming nuclei concentration leads to changes in hail sizes, which
 429 are known to have a great impact on the dynamic, thermodynamic and pre-
 430 cipitation characteristics of the resulting storm (van den Heever and Cotton,
 431 2004).

432 Some studies on the effects of dust on the masses of various ice species within
 433 the anvils of convective storms during CRYSTAL-FACE dedicated to the
 434 Florida convection have been performed by van den Heever et al. (2006) and
 435 Carrio et al. (2007). These studies used the mesoscale model RAMS, which
 436 includes simple a parameterization for connecting the concentration of CCN
 437 and IFN and the nucleated droplets and ice crystals. These studies have
 438 shown that IFN concentrations have a greater impact on updraft strength
 439 during the mature and dissipating storm stages.

440 Moreover, a recent study based on satellite and direct aircraft measurement
 441 during NAMMA (a part of AMMA operated by NASA) supports the hypoth-
 442 esis that Saharan dust may have led to invigoration of rain bands associated
 443 with tropical cyclogenesis near West African coastline (Jenkins et al., 2008).
 444 Another recent study (Min et al., 2009), that uses some multi-platform and

445 multi-sensor observations, shows that the consequences of dust on a particu-
 446 lar MCS observed over the Gulf of Guinea were to shift the precipitation size
 447 spectrum from heavy rain to light rain. At this stage several questions arise
 448 on the particular properties of MCS formed over semi-arid regions: (1) Are
 449 anvil lifetimes and spatial dimensions affected by the dust aerosols generated
 450 by downdrafts? (2) Does a feedback exist between dust and precipitation
 451 by limiting the ice sedimentation in the upper troposphere? On the one
 452 hand observations alone cannot answer these questions due to the difficul-
 453 ties of de-aliasing the meteorological particularities of each MCS. On the
 454 other hand, mesoscale models need to improve their parameterization of ice
 455 microphysics processes to include a realistic scheme of ice activation before
 456 sensitivity studies on ice nuclei impacts can be performed. One goal of the
 457 AMMA field campaign was to improve the knowledge of the properties of
 458 the West African MCS. The goal of this study was to show that a MCS
 459 over a semi-arid region can create high concentration of ice nuclei in the up-
 460 per troposphere. A joint investigation using both observations and models
 461 can serve to further understanding how aerosols can impact significantly the
 462 microphysics and the dynamics of an MCS in semi-arid region.

8. acknowledgments

The authors wish to thanks Jean-Pierre Chaboureau for providing the
 MSG brithness temperature pictures. MSG observations were obtained from
 Météo-France/Centre de Météorologie Spatiale through AMMASAT. Based
 on a French initiative, AMMA was built by an international scientific group
 and is currently funded by a large number of agencies, especially from France,

UK, US and Africa. It has been the beneficiary of a major financial contribution from the European Community's Sixth Framework Research Program. Detailed information on scientific coordination and funding is available on the AMMA international website <http://www.amma-international.org>.

References

- Albrecht, B., 1989. Aerosols, cloud microphysics, and fractional cloudiness. *Science* 245, 1227–1230.
- Alfaro, S., Gomes, L., 2001. Modeling mineral aerosol production by wind erosion: Emission intensities and aerosol size distributions in source areas. *J. Geophys. Res.* 106 (D16), 18075–18084.
- Andronache, C., 2003. Estimated variability of below-cloud aerosol removal by rainfall for observed aerosol size distributions. *Atmos. Chem. Phys.* 3, 131–143.
- Barthe, C., Molini, G., Pinty, J., 2005. Description and first results of an explicit electrical scheme in a 3d cloud resolving model. *Atmos. Res.* 76, Issues 1-4, 95–113.
- Bechtold, P., Bazile, E., Guichard, F., Mascart, P., Richard, E., 2001. A mass-flux convection scheme for regional and global models. *Quart. J. Roy. Meteor. Soc.* 127, 869–886.
- Bougeault, P., Lacarrere, P., 1989. Parametrization of orography-induced turbulence in a meso-beta model. *Mon. Wea. Rev.* 117, 1872–1890.

- BouKaram, D., Flamant, C., Knippertz, P., Reitebuch, O., Chong, M., Pelon, J., Dabas, A., 2008. Dust emissions over the sahel associated with the west african monsoon inter-tropical discontinuity region: a representative case study. *Quart. J. Roy. Meteor. Soc.* 134, 621–634.
- Caniaux, G., Redelsperger, J., Lafore, J., 1994. A numerical study of the stratiform region of a fast-moving squall line. part i general description and water and heat budgets. *J. Atmos. Sci.* 51, 2046–2074.
- Carrio, G., van den Heever, S., Cotton, W., 2007. Impacts of nucleating aerosol on anvil-cirrus clouds: A modeling study. *Atm. Res.* 84, 111–131.
- Chaboureaud, J., Pinty, J., 2006. Validation of a cirrus parameterization with meteosat second generation observations. *Geophysical Res. Let.* 33, doi:10.1029/2005GL024725.
- Chin, M., Rood, R., Lin, S. J., Muller, J. F., Thompson, A., 2000. Atmospheric sulfur cycle simulated in the global model gocart: Model description and global properties. *J. Geophys. Res.* 105, 24,671–24,687.
- Chomette, O., Legrand, M., Marticorena, M., 1999. Determination of the wind speed threshold for the emission of desert dust using satellite remote sensing in the thermal infrared. *J. Geophys. Res.* 104, 24,671–24,687.
- Cohard, J., Pinty, J., 2000. A comprehensive two-moment warm microphysical bulk scheme . ii : 2d experiments with a non hydrostatic model. *Quart. J. Roy. Meteor. Soc.* 126, 1843–1859.
- Crumevrolle, S., Gomes, L., Tulet, P., Matsuki, A., Schwarzenboeck, A., Crahan-Kaku, K., 2008. Increase of the aerosol hygroscopicity by cloud

- processing in a mesoscale convective system: a case study from the amma campaign. *Atmos. Chem. Phys.* 8 (23), 6907–6924.
- DeMott, P., Sassen, K., Poellot, M., Baumgardner, D., Rogers, D., Brooks, S., Prenni, A., Kreidenweis, S., 2003. African dust aerosols as atmospheric ice nuclei. *Geophysical Res. Let.* 30 (14), 1732, doi:10.1029/2003GL017410.
- Flamant, C., Chaboureaud, J., Parker, D., Taylor, C., Cammas, J., Bock, O., Timouke, F., Pelon, J., 2007. Airborne observations of the impact of a convective system on the planetary boundary layer thermodynamics and aerosol distribution in the inter-tropical discontinuity region of the west african monsoon. *Quart. J. Roy. Meteor. Soc.* 133, 1175–1189.
- Flamant, C., Knippertz, P., Parker, D., Chaboureaud, J., Lavaysse, C., Agusti-Panareda, A., Kergoat, L., 2009. The impact of a mesoscale convective system cold pool on the northward propagation of the intertropical discontinuity over west africa. *Quart. J. Roy. Meteor. Soc.* 135, 139–159.
- Gilmore, M., Straka, J. M., Rasmussen, E. N., 2004a. Precipitation and evolution sensitivity in simulated deep convective storms: Comparisons between liquid-only and simple ice and liquid phase microphysics. *Mon. Wea. Rev.* 132, 1897–1946.
- Gilmore, M., Straka, J. M., Rasmussen, E. N., 2004b. Precipitation uncertainty due to variations in precipitation particle parameters within a simple microphysics scheme. *Mon. Wea. Rev.* 132, 2610–2627.
- Ginoux, P., Chin, M., Tegen, I., Prospero, J., Holben, B., Dubovik, O., Lin,

- S.-J., 2001. Sources and distributions of dust aerosols simulated with the gocart model. *J. Geophys. Res.* 106, 20255.
- Grini, A., Tulet, P., Gomes, L., 2006. Dusty weather forecast using the mesonh atmospheric model. *J. Geophys. Res.* 111, doi:10.1029/2005JD007007.
- Houghton, J., Ding, Y., Griggs, D. J., Noguer, M., van der Linden, P. J., Dai, X., Maskell, K., Johnson, C. A. (Eds.), 2001. *IPCC 2001: Climate Change 2001*. Cambridge University Press, Cambridge, England.
- IPCC (Ed.), 2007. *Climate change 2007: The scientific basis. Contribution of working group I to the Fourth Assessment Report of the Intergovernmental Panel on Climate Change*. <http://www.ipcc.ch/>.
- Jenkins, G., Pratt, A., Heymsfield, A., 2008. Possible linkages between saharan dust and tropical cyclone rain band invigoration in the eastern atlantic during namma-06. *Geophysical Res. Let.* 35, doi:10.1029/2008GL034072.
- Kanji, Z., Abbatt, J., 2006. Laboratory studies of ice formation via deposition mode nucleation onto mineral dust and n-hexane soot samples. *J. Geophys. Res.* 111, doi:10.1029/2005JD006766.
- Knippertz, P., Trentmann, J., Seifert, A., 2009. High-resolution simulations of convective cold pools over the northwestern sahara. *J. Geophys. Res.* 114 (D08110), doi:10.1029/2008JD011271.
- Lafore, J., Stein, J., Asencio, N., Bougeault, P., Ducrocq, V., Duron, J., Fischer, C., Hereil, P., Mascart, P., Pinty, V. M. J., Redelsperger, J., Richard,

- E., de Arellano, J. V.-G., 1998. The meso-nh atmospheric simulation system. part i: adiabatic formulation and control simulations. *Ann. Geophys.* 16, 90–109.
- Levin, Z., Ganor, E., Gladstein, V., 1996. The effects of desert particles coated with sulfate on rain formation in the eastern mediterranean. *Journal of Applied Meteorology* 35, 1511–1523.
- Lin, Y., Farley, R., Orville, H., 1983. Bulk parameterization of the snow field in a cloud model. *J. Climate Appl. Meteor.* 22, 1065–1092.
- Lohmann, U., Diehl, D., 2006. Sensitivity studies of the importance of dust ice nuclei for the indirect aerosol effect on stratiform mixed-phase clouds. *J. Atmos. Sci.* 63, 968–982.
- Marshall, J., Parker, D., Grams, C., Haywood, J., 2008. Uplift of saharan dust south of the intertropical discontinuity. *J. Geophys. Res.* 113 (D21102), doi:10.1029/2008JD009844.
- Martcorena, B., Bergametti, G., 1995. Modeling of the atmospheric dust cycle: 1. design of a soil derived dust emission scheme. *J. Geophys. Res.* 100, 16415–16429.
- Masson, V., 2000. A physically-based scheme for the urban energy balance in atmospheric models. *Boundary-Layer Meteorology* 94, 357–397.
- Min, Q., Li, R., Lin, B., Joseph, E., Wang, S., Hu, Y., Morris, V., Chang, F., 2009. Evidence of mineral dust altering cloud microphysics and precipitation. *Atmos. Chem. Phys.* 9, 3223–3231.

- Nelson, J., 2001. Growth mechanisms to explain the primary and secondary habits of snow crystals. *Phil. Mag. A* 81, 10, 2337–2373.
- Noilhan, J., Mahfouf, J., 1996. The isba land surface parameterization scheme. *Global and Plan. Change* 13, 145–159.
- Pinty, J., Jabouille, P., 1998. A mixed-phase cloud parameterization for use in mesoscale non hydrostatic model: simulations of a squall line and of orographic precipitations. *Conference of Cloud Physics* Everett, WA, USA, 217–220.
- Prenni, A., DeMott, P., Twohy, C., Poellot, M., Kreidenweis, S., Rogers, D., Brooks, S., Richardson, M., Heymsfield, A., 2007. Examinations of ice formation processes in florida cumuli using ice nuclei measurements of anvil ice crystal particle residues. *J. Geophys. Res.* 112 (D10221), doi:10.1029/2006JD007549.
- Pruppacher, H., Klett, J., 2000. *Microphysics of clouds and precipitation*. Kluwer academic publishers.
- Redelsperger, J., Thorncroft, D., A.Diedhiou, Lebel, T., Parker, D., Polcher, J., 2006. African monsoon multiplidisciplinary analysis: An international research project and field campaign. *Bull. Am. Met. Soc.* 87, 1739–1746.
- Richardson, M., DeMott, P., Kreidenweis, S., Cziczo, D., Dunlea, E., Jimenez, J., Thomson, D., Ashbaugh, L., Borys, R., Westphal, D., Casuccio, G., Lersch, T., 2007. Measurements of heterogeneous ice nuclei in the western united states in springtime and their relation to aerosol characteristics. *J. Geophys. Res.* 112 (D02209), doi:10.1029/2006JD007500.

- Sandu, I., Brenguier, J.-L., Geoffroy, O., Thouron, O., Masson, V., 2008. Aerosol impacts on the diurnal cycle of marine stratocumulus. *J. Atmos. Sci.* 65, 2705–2718, doi:10.1175/2008JAS2451.1.
- Seinfeld, J., Pandis, S., 1997. *Atmospheric Chemistry and Physics*. Wiley interscience pub.
- Slinn, W., 1983. *Atmospheric sciences and power production* 1979. Precipitation Scavenging, U.S. Department of Energy, Washington, D.C., chap. 11.
- Suhre, K., Mari, C., Bates, T., Johnson, J., Rosset, R., Wang, Q., Bandy, A., Blake, D., Businger, S., Eisels, F., Huebert, B., Kok, G., Mauldin, R. I., Prévôt, A., Schillawski, R., Tanner, D., Thornton, D., 1998. Physico-chemical modeling of the first aerosol characterization experiment (ace 1) lagrangian b, 1. a moving column approach. *J. Geophys. Res.* 103, 16433–16455.
- Tegen, I., Lacis, A. A., 1996. Modeling of particle size distribution and its influence on the radiative properties of mineral dust aerosol. *J. Geophys. Res.* 101, 19237–19244.
- Tost, H., Jockel, P., Kerkweg, A., Sander, R., Lelieveld, J., 2006. Technical note: A new comprehensive scavenging submodel for global atmospheric chemistry modelling. *ACP* 6, 565–574.
- Tulet, P., Crassier, V., Cousin, F., Shure, K., Rosset, R., 2005. Orilam, a three moment lognormal aerosol scheme for mesoscale atmospheric model.

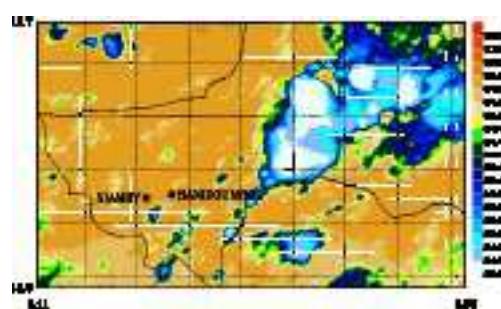
- on-line coupling into the mesonh-c model and validation on the escompte campaign. *J. Geophys. Res.* 110, doi:10.1029/2004JD005716.
- Tulet, P., Crassier, V., Solmon, F., Guedalia, D., Rosset, R., 2003. Description of the mesoscale nonhydrostatic chemistry model and application to a transboundary pollution episode between northern france and southern england. *J. Geophys. Res.* 108, D1, 4021.
- Tulet, P., Grini, A., Griffin, R., Petitcol, S., 2006. Orilam-soa: A computationally efficient model for predicting secondary organic aerosols in 3d atmospheric models. *J. Geophys. Res.* 111, doi:10.1029/2006JD007152.
- Twomey, S., 1959. The nuclei of natural cloud formation. part ii: The supersaturation in natural clouds and the variation of cloud droplet concentration. *Pure Appl. Geophys.* 43, 243–249.
- van den Heever, S., Carrio, G., Cotton, W., Demott, P., Prenni, A., 2006. Impacts of nucleating aerosol on florida storms. part i: Mesoscale simulation. *J. Atmos. Sci.* 61, 1596–1609.
- van den Heever, S., Cotton, W., 2004. The impact of hail size on simulated supercell storms. *J. Atmos. Sci.* 63, 1752–1775.
- Zender, C., Bian, H., Newman, D., 2003. The mineral dust entrainment and deposition (dead) model: Description and global dust distribution. *J. Geophys. Res.* 108 (D14), 4416, <http://dust.ess.uci.edu/dead/>.

List of Figures

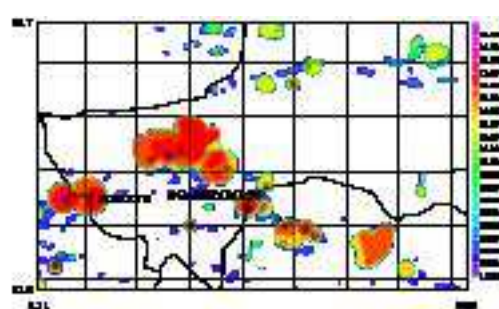
- 1 Brightness temperature from the MSG satellite (channel 10.8 μm , in K, color scale on the right), 1 July, 2006 at 18UTC (a), 2 July, 2006 at 00 UTC (c) and 2 July, 2006 at 02 UTC (e). Cloud top altitude (in km, color scale on the right) and instantaneous precipitation (isolines at 5, 25, 50, 75 $mm.h^{-1}$) simulated by MesoNH on 1 July, 2006 at 17 UTC (b), 20 UTC (d) and 22 UTC (f). 33
- 2 Dust mass concentration ($\mu g.m^{-3}$) at the surface (colors, scale on the right) and 10 meter wind fields (arrows) simulated by MesoNH (SCAV) on 1 July, 2006 at 20 UTC. The solid line represents the vertical cross section of Figures 3, 4, 5 and 6. . . 33
- 3 The vertical cross section of total condensate mixing ratio (shade in gkg^{-1} , scale on right) on 1 July at 20 UTC. Red isolines correspond to the mixing ratio of rain water (at 0.25, 0.75, 1.25, 2. 3. and 4. gkg^{-1}) and black isolines to the vertical velocity (dotted for subsidence at 1 and 0.5 ms^{-1} and solid lines for ascent motion at 1, 2, 5, 10, 15 and 20 ms^{-1}). At the bottom: the distance (in km) of the vertical cross section plotted on Figure 2 (the origin corresponds to the south west point). 33

- 4 The vertical cross section between 0 and 3000 m agl of simulation SCAV on 1 July at 20 UTC: (a) potential temperature (in K, color scale on the right), wind stream lines (solid lines with arrows) and kinetic turbulent energy (shaded, scale on the top); (b) dust mass concentration (in $\mu g.m^{-3}$, color scale on the right) and rain water mixing ratio (shaded, scale on the top). At the bottom: the distance (in km) of the vertical cross section plotted on Figure 2 (the origin corresponds to the south west point). 33
- 5 The vertical cross section of dust mass concentration on 1 July at 20 UTC of simulation NOSCAV ($\mu g.m^{-3}$, scale on right). At the bottom: the distance (in km) of the vertical cross section plotted on Figure 2 (the origin corresponds to the south west point). 33
- 6 The vertical cross section of the difference of dust mass concentration between NOSCAV and SCAV simulations ($\mu g.m^{-3}$, scale on right) on 1 July at 20 UTC. The dashed line corresponds to the vertical profile plotted in Figure 7. At the bottom: the distance (in km) of the vertical cross section plotted on Figure 2 (the origin corresponds to the south west point). . 34

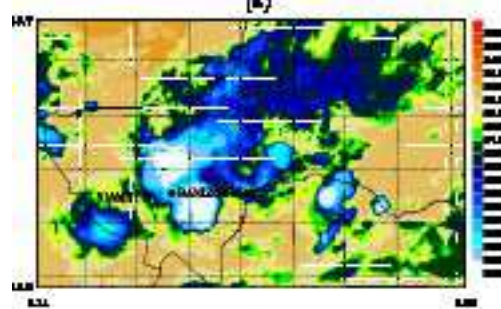
7	A vertical profile in the convective region of the MCS simulated by MesoNH on 1 July, 2006 at 20 UTC on the cross-section indicated by the dashed line of Figure 6. Mass concentration (a) ($\mu g.m^{-3}$) and particles number concentration (b)(cm^{-3}) for modes at $R_g = 0.32\mu m$ (in green), $R_g = 1.73\mu m$ (in red) and $R_g = 4.33\mu m$ (in blue). The solid line represents the simulation SCAV and dashed line represents the simulation NOSCAV.	34
8	Dust number concentration (cm^{-3} , scale on right) of simulation SCAV, on July, 2 at 00 UTC at 16,000 m agl (a) and at 20,000 m agl (b).	34



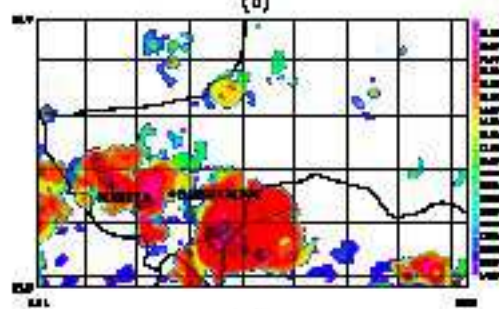
(a)



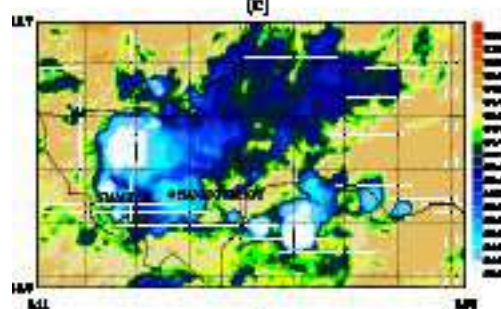
(b)



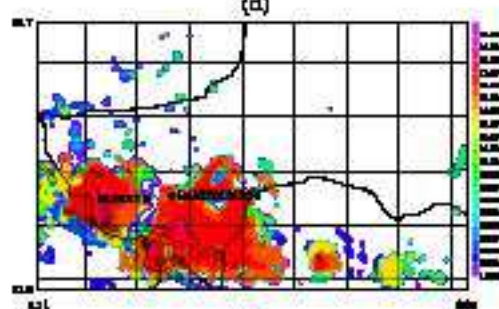
(c)



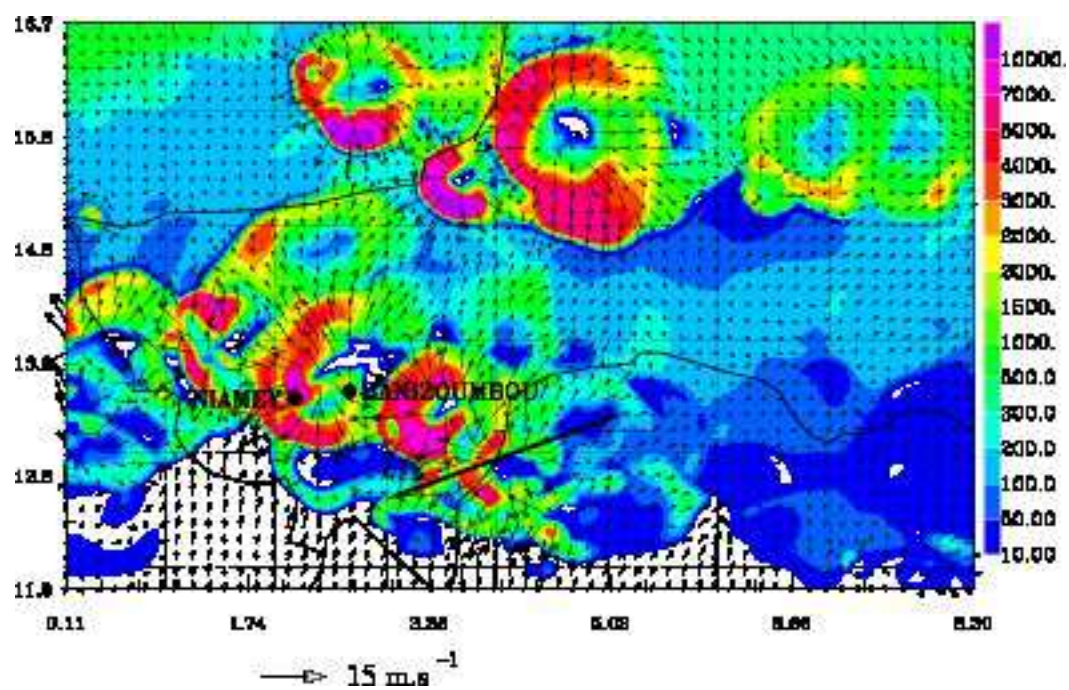
(d)

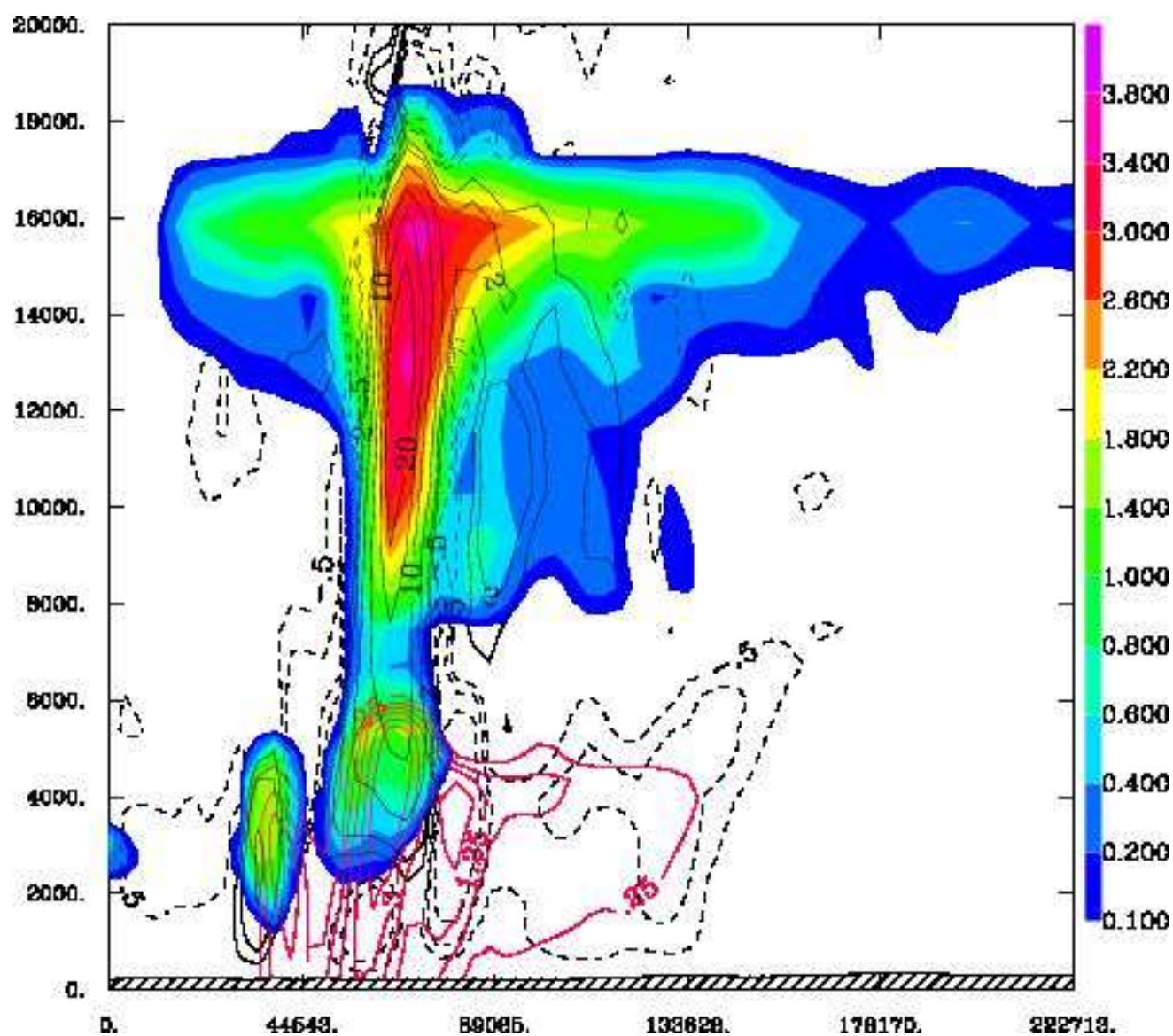


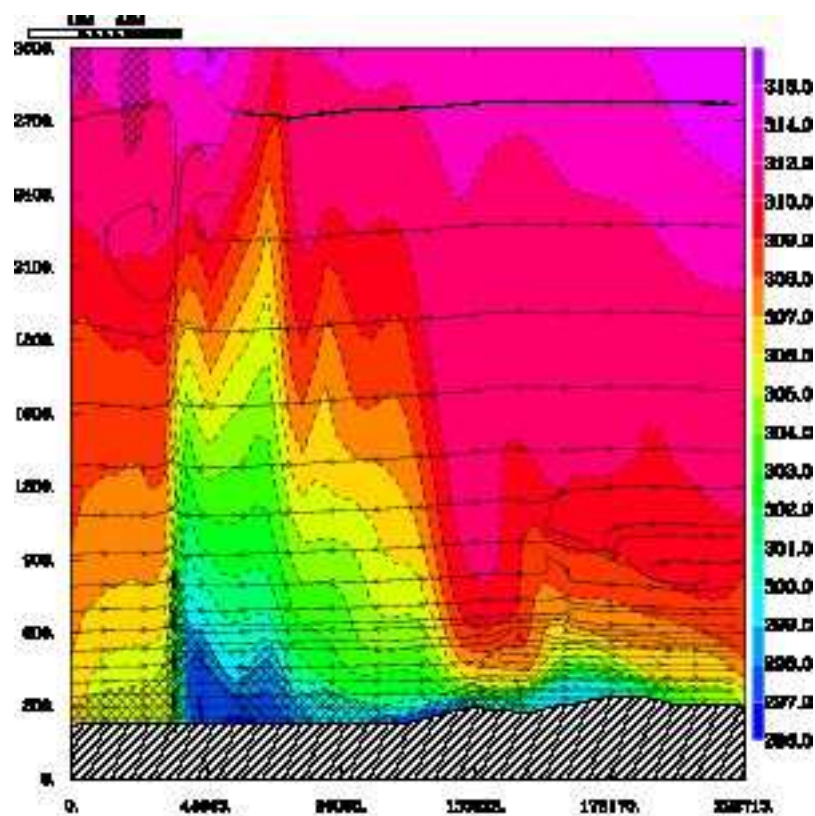
(e)



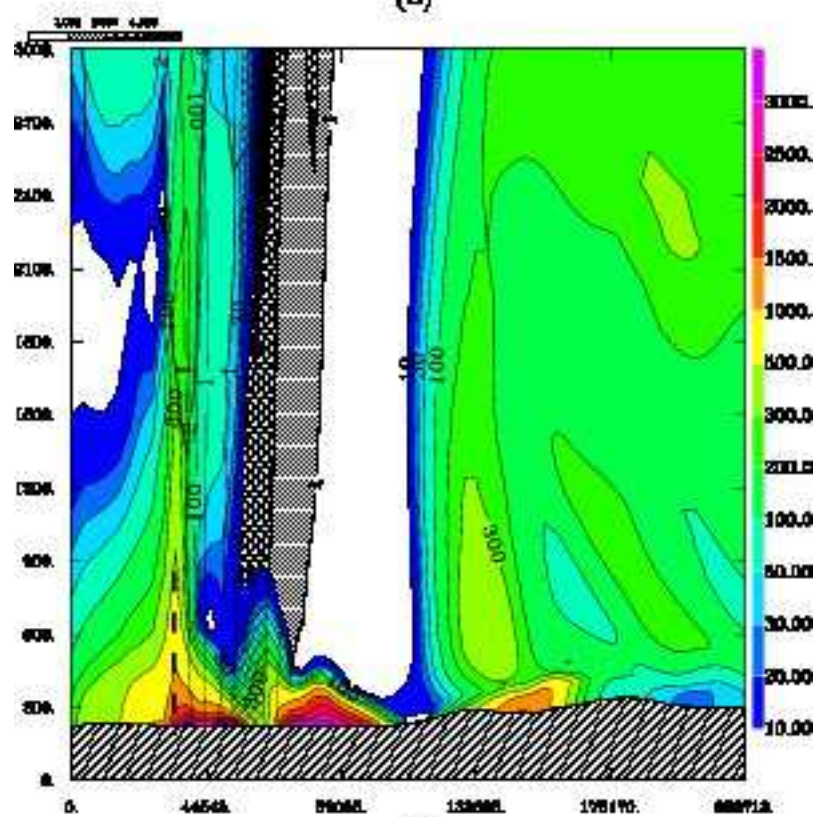
(f)



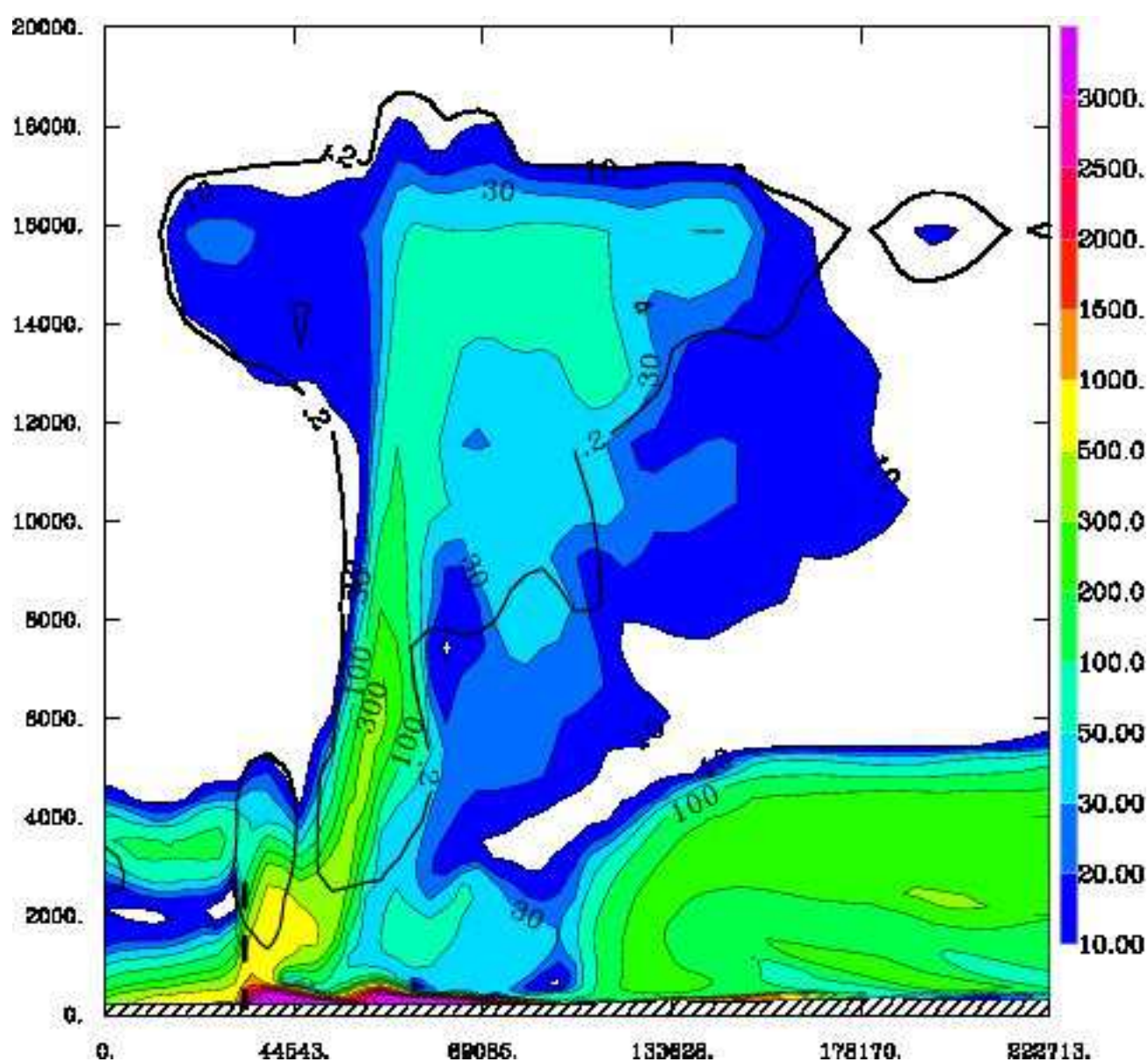


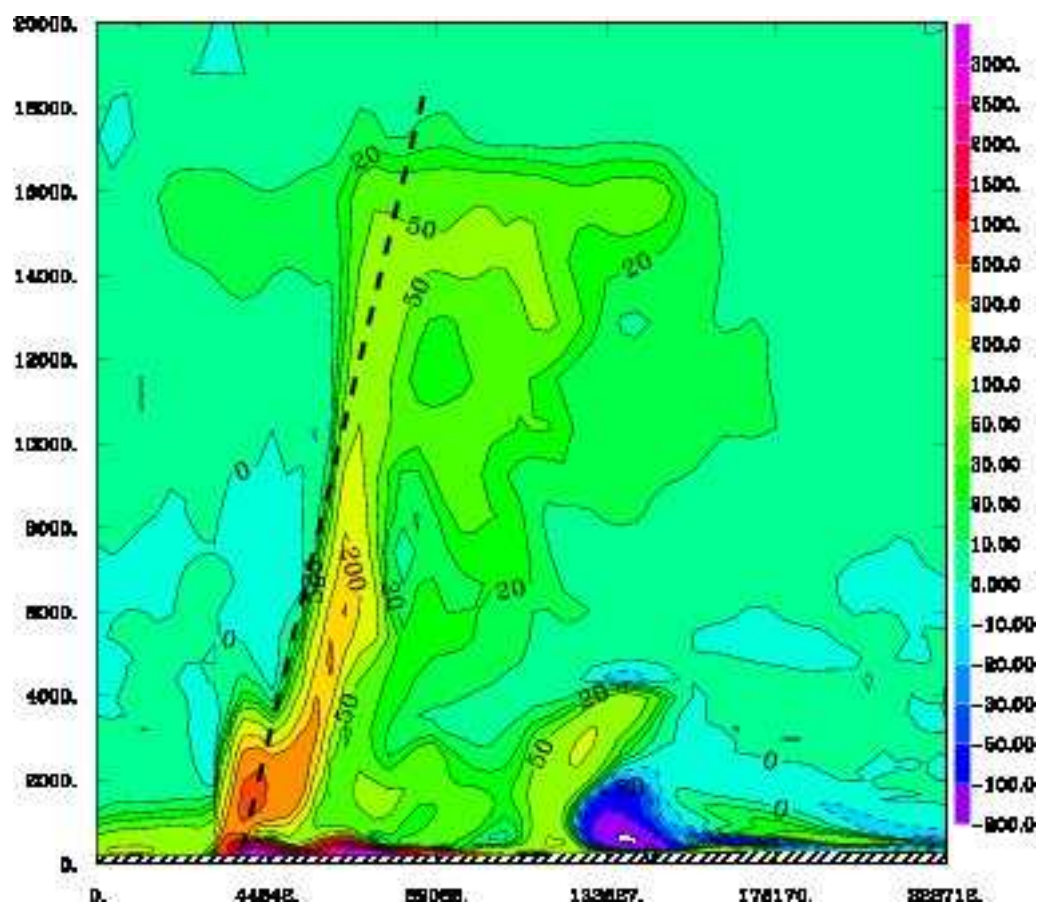


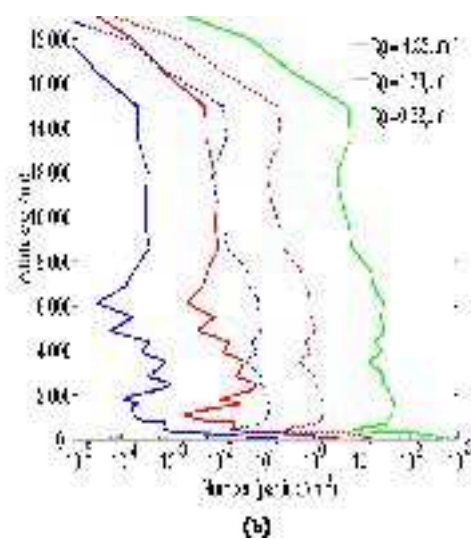
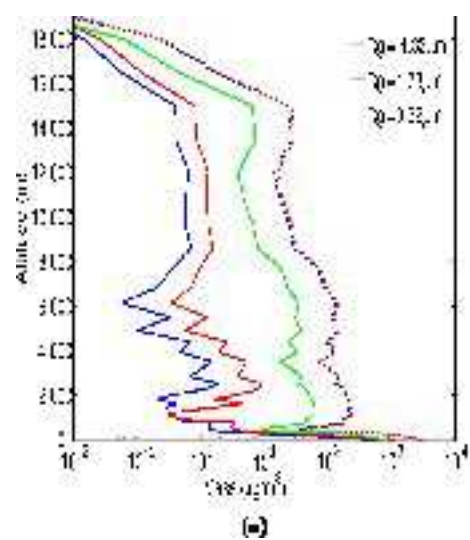
(a)

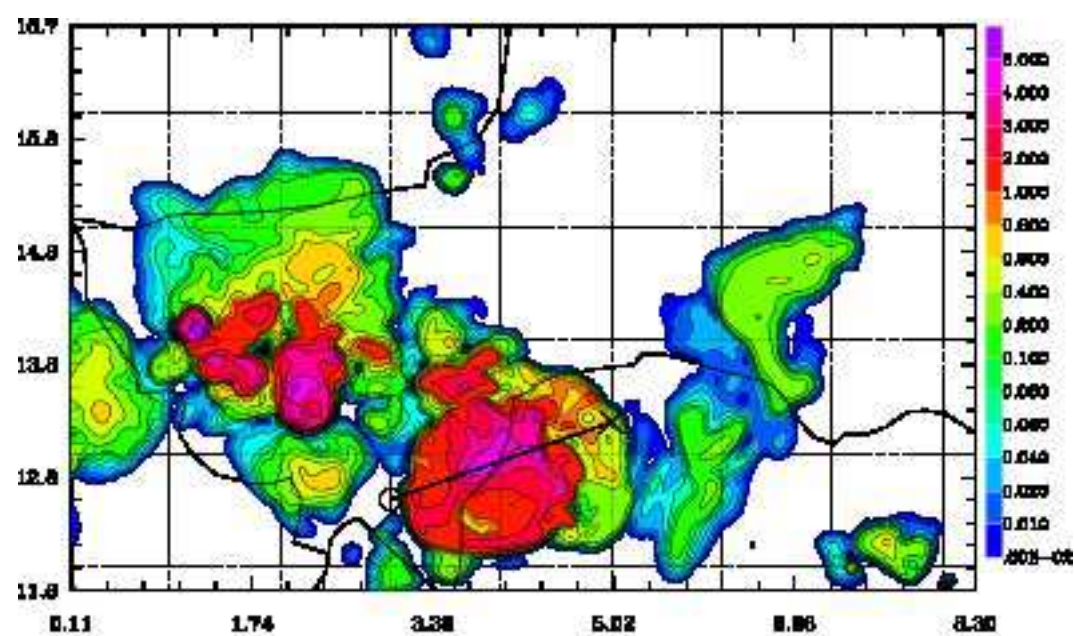


(b)

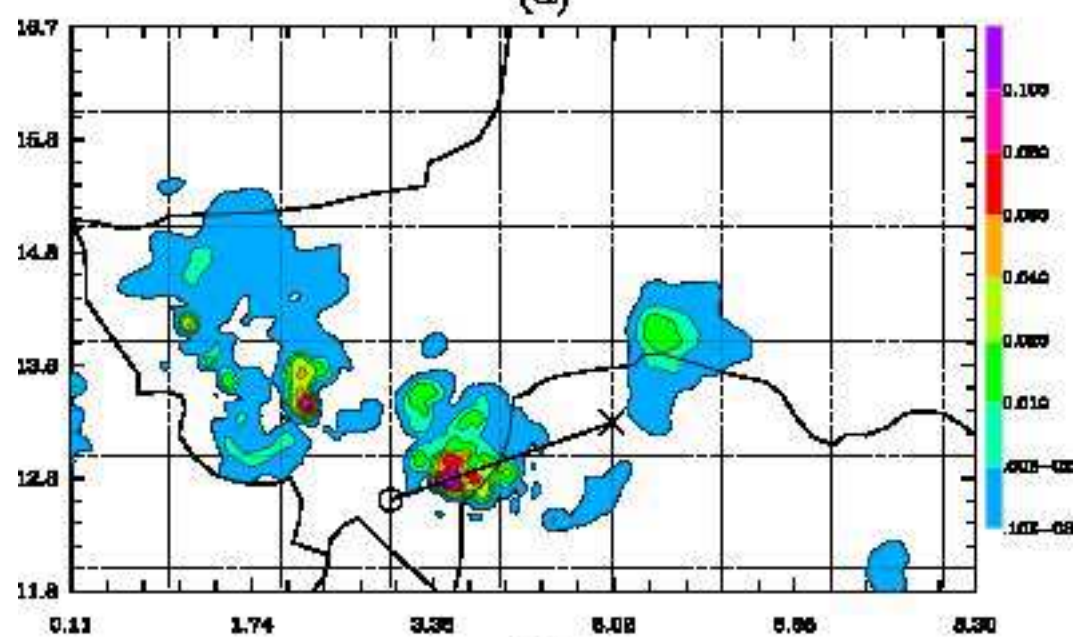








(a)



(b)